Deep-Sea Research I, Vol 40 No 7 pp 1365–1377, 1993
Printed in Great Britain

0967–0637/93 $6 00 + 0 00

The mesoscale eddy field of the Middle Adriatic Sea during fall 1988

ELIO PASCHINI,* ANTONIO ARTEGIANI* and NADIA PINARDI†

(*Received* 30 *November* 1990, *in revised form* 6 *October* 1992, *accepted* 6 *October* 1992)

Abstract—The analysis of the first mesoscale experiment in the middle Adriatic Sea reveals the horizontal and vertical scale of the eddy field The mesoscale variability is characterized by 10–20 km in diameter eddies. They are lower thermocline intensified, and the velocities in the upper and lower thermocline levels range from 10 to 1 cm s^{-1}, respectively The eddies are small because of the local Rossby radius of deformation (5.4 and 2.8 km for the first and second internal baroclinic mode, respectively) and because they are second baroclinic mode intensified The Levantine Intermediate Water is found in tongue-like features intruding between the intense eddy field

INTRODUCTION

THE Adriatic Sea (Fig.1) is an elongated semi-enclosed basin located in the northern part of the eastern Mediterranean Sea between Italy and Yugoslavia. The northern Adriatic is a shallow continental shelf of average depth of about 35 m, which smoothly deepens in the central part; the southern Adriatic has an abyssal basin of about 1200 m and is connected to the Ionian Sea through the Strait of Otranto with a sill of more than 800 m. The middle Adriatic Sea is characterized by two depressions, the western and eastern Pomo depressions, deeper than 200 m, connected to the southern Adriatic with a sill of about 170 m.

The Adriatic Sea has been widely studied in the past because of important deep water convection processes occurring during winter in its northern part (ZORE-ARMANDA, 1963; ARTEGIANI and SALUSTI, 1987) and in its southern part (POLLAK, 1951; OVCHINNIKOV *et al.*, 1987). Furthermore, the general circulation of the two regions has been described (ZORE-ARMANDA, 1963) with particular attention to the northern Adriatic region (FRANCO *et al.*, 1982; MALANOTTE-RIZZOLI and BERGAMASCO, 1983). From these studies the general circulation is known to consist of several cyclonic gyres during winter. In all seasons, the middle and southern Adriatic general circulation surface currents consist of a smooth flow encircling the whole basin, entering from Otranto and following the Yugoslavian coasts. Following the 100 m isobath, this flow turns southward along the Italian coasts approximately at the northern border of our study area (see Fig. 1). There is evidence that during summer–autumn conditions this flow splits into two separate cyclonic gyres in the middle

*Istituto di Ricerche sulla Pesca Marittima - CNR, Ancona, Italy.
†Istituto per lo studio delle Metodologie Geofisiche Ambientali, Modena, Italy

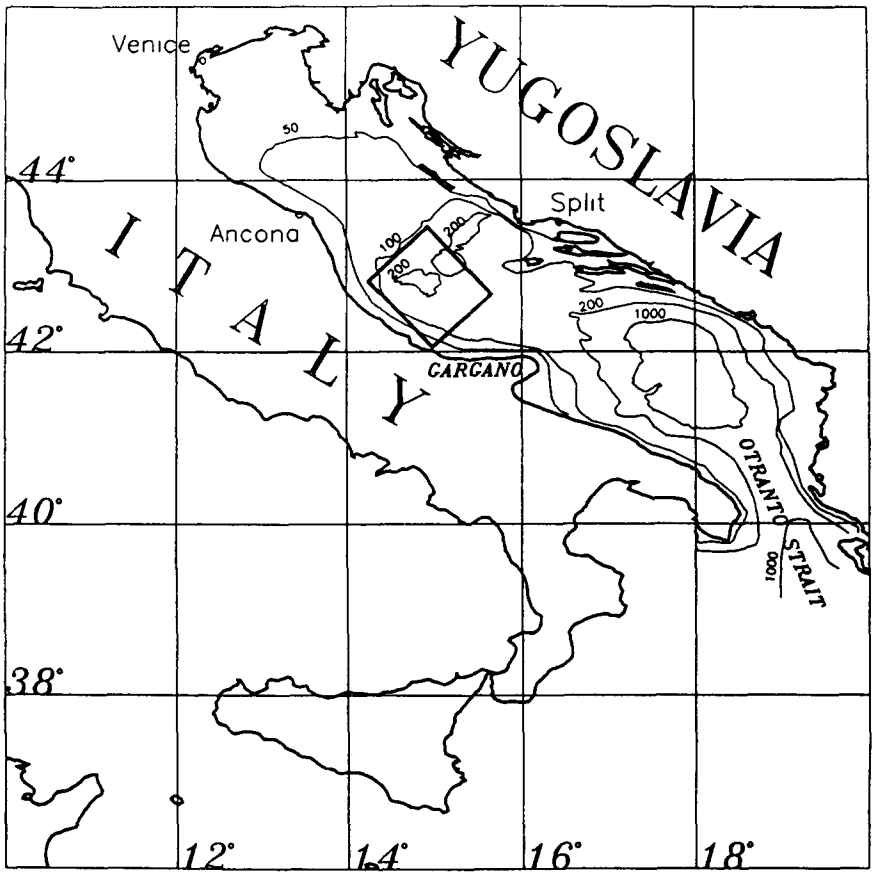

Fig 1. The Adriatic Sea coastlines with the bathymetric contours The thick line box indicates the region of the CTD survey

and southern Adriatic regions. The return flow along the Italian coasts is intensified (ZORE-ARMANDA, 1956) and at a depth of about 100 m forms a thin bottom boundary current carrying the dense water formed during the winter in the northern Adriatic (ARTEGIANI *et al.*, 1989).

Evidence for the mesoscale signal and its energetic contribution to the local current system for both winter and summer conditions was noted in large-scale surveys carried out during the sixties (HENDERSHOTT and RIZZOLI, 1972; FRANCO, 1972) and recent previous cruises (ZORE-ARMANDA and GACIC, 1987; ARTEGIANI *et al.*, 1987). However, the mesoscale variability is practically unknown because of the accuracy required in sampling its spatial scales and the need for both salinity and temperature measurements.

In this article we discuss the first successful mesoscale experiment carried out in the middle Adriatic Sea. We analyse a mesoscale resolution hydrographic data set taken in the region of the middle Adriatic, and we connect these measurements to the previously known general circulation flow.

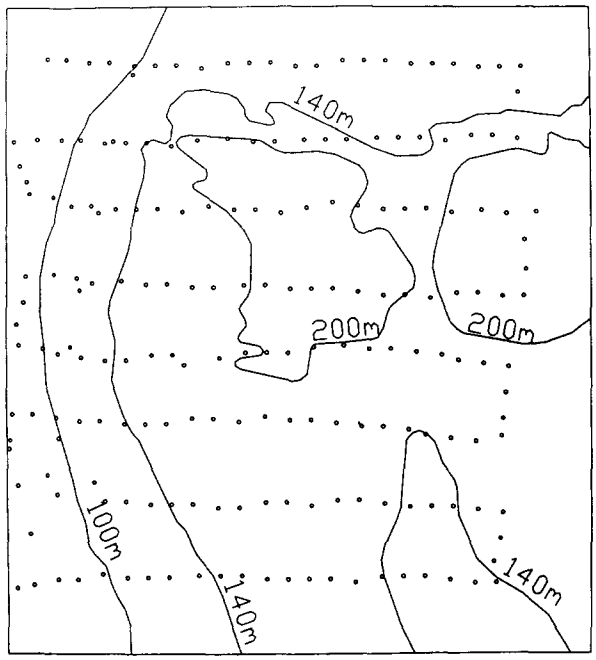

Fig 2 CTD station locations superimposed on local bathymetry. The box corresponds to the domain of the objective analysis mapping The domain is a box 90 × 100 km^2, rotated 42° anticlockwise and centered at 14.95°E, 42.73°N

THE DATA SET

The data set consists of 196 casts taken with a Neil Brown Mk III CTD on board the R.V. *S. Lo Bianco* (Fig. 2). They were collected during a period of 4 days starting from 7 November 1988. The CTD was calibrated at the Saclant Center Laboratory (La Spezia, Italy) and the accuracy is ±1.6 dbar for pressure, ±0.005°C and ±0.005 mmho for temperature and conductivity measurements, respectively. The stations occupy the western Pomo depression and only partially occupy the eastern one, covering an area of 90 × 100 km^2. The box in Fig. 2 represents the domain of interpolation used in the objective mapping of the physical fields.

The strategy of sampling used in this cruise has been proved to be robust to resolve the mesoscale fields of other world regions (Mooers and Robinson, 1984; Robinson *et al.*, 1987). It consists of highly resolved measurements at the nominal distance of 2 miles along several transects; on the other hand, the transects are separated by a distance of 6 miles. This allows a fast coverage of the region to obtain a quasi-synoptic data set (4 days in this case). The raw data were converted to practical salinity and averaged every decibar (Unesco, 1988).

WATER MASS ANALYSIS AND QUASIGEOSTROPHIC VERTICAL MODES

To define the local water mass properties of the region, we have averaged the T, S profiles between all the stations and calculated the standard deviations. The results are shown in Fig. 3.

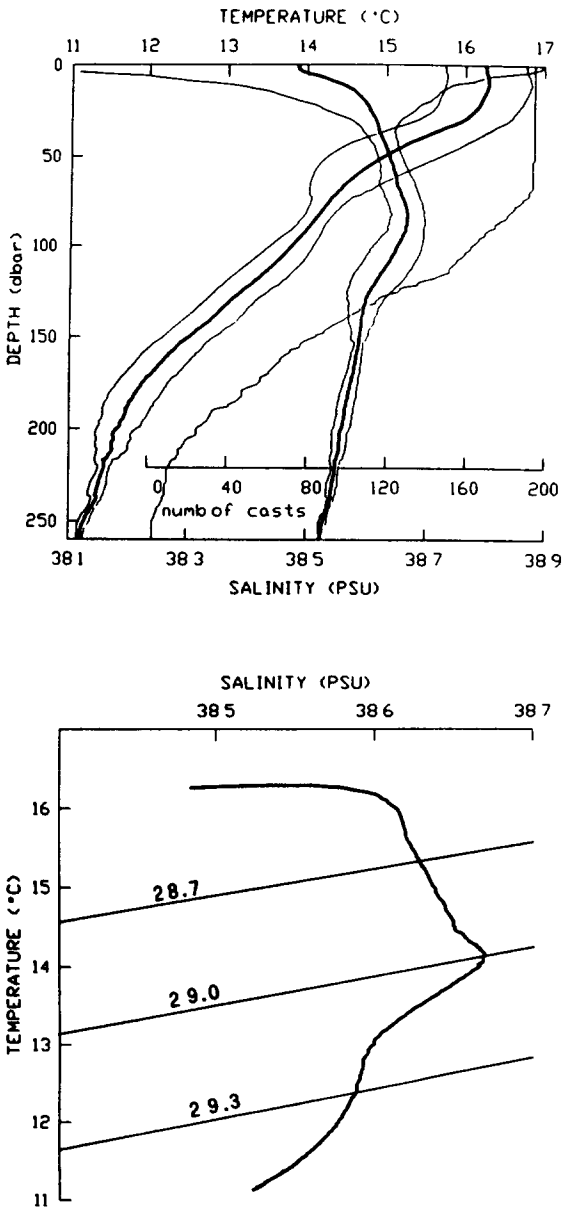

Fig. 3. Upper panel: stations average temperature and salinity profiles (darker lines) as a function of depth enclosed between curves of 1 S.D The thin third profile indicates the number of casts used in the average as a function of depth. Lower panel: *T–S* diagram for the stations average profiles shown in the upper panel

The profiles can be divided into three vertical regions corresponding to different gradients in the T, S profiles. The first, between the surface and 30 m, is characterized by a temperature mixed layer that is partially eroded at its bottom. In the upper 10 m there is a layer of less saline and cooler waters of coastal origin, but we do not separate them from

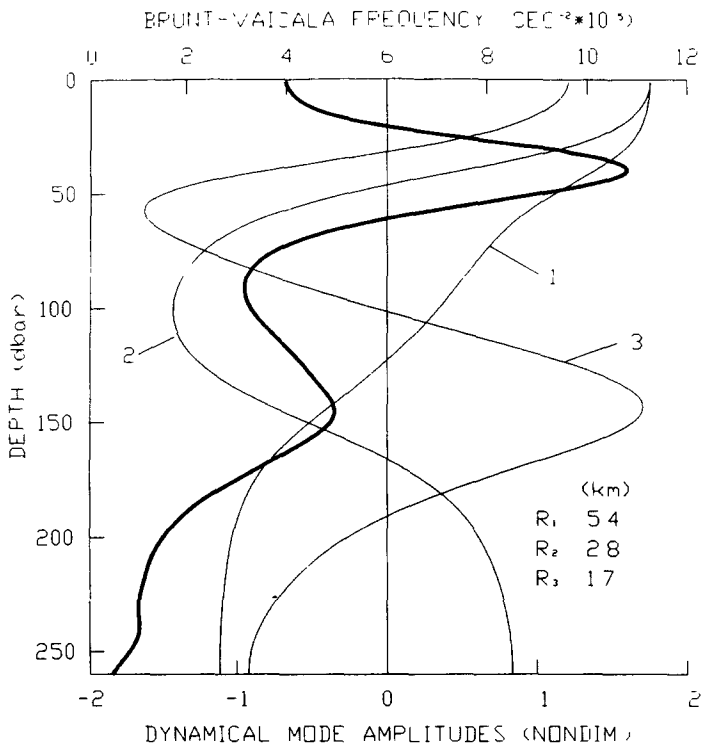

Fig 4. Squared Brunt–Vaisala frequency profile calculated from the average T and S profiles shown in Fig 2 (dark line). Baroclinic quasigeostrophic vertical modes calculated from the Brunt–Vaisala profile 1, 2 and 3 indicate the first three internal baroclinic modes with their respective Rossby radii.

the mixed temperature layer. We indicate this region simply as the surface water region (SW) affected by strong air–sea interactions and coastal waters.

The second region, located between 30 and 130 m, shows a smooth decrease in the temperature profile, while the salinity reaches a subsurface maximum at about 80–90 m. The waters belonging to this region are called Levantine Intermediate Waters (LIW) because of their subsurface salinity maximum. They are formed in the eastern Levantine basin (Ovchinnikov, 1984; Hecht *et al.*, 1988; Özsoy *et al.*, 1989) and they are presumably advected into this region. Due to horizontal and vertical mixing, they are locally characterized by salinity values >38.6 PSU, while in the region of their formation they attain a value >38.9 PSU. In the LIW region the temperature decreases almost linearly from 16 to 13°C with no significant changes in the slope at the level of maximum salinity.

The third region, located between 140 m and the bottom of the basin, is characterized by very dense waters ($11 < T < 13$°C and $38.5 < S < 38.6$ PSU) probably formed in the northern Adriatic by deep winter mixing processes and sunk in this region on their way to the Ionian Sea. We call this region the deep water (DW) region.

The T–S diagram of Fig. 3 shows very clearly the three different water masses: the SW of low salinity, above 16°C; the LIW between 13 and 16°C and with salinity values >38.6 PSU; the DW below 13°C and with salinity <38.6 PSU.

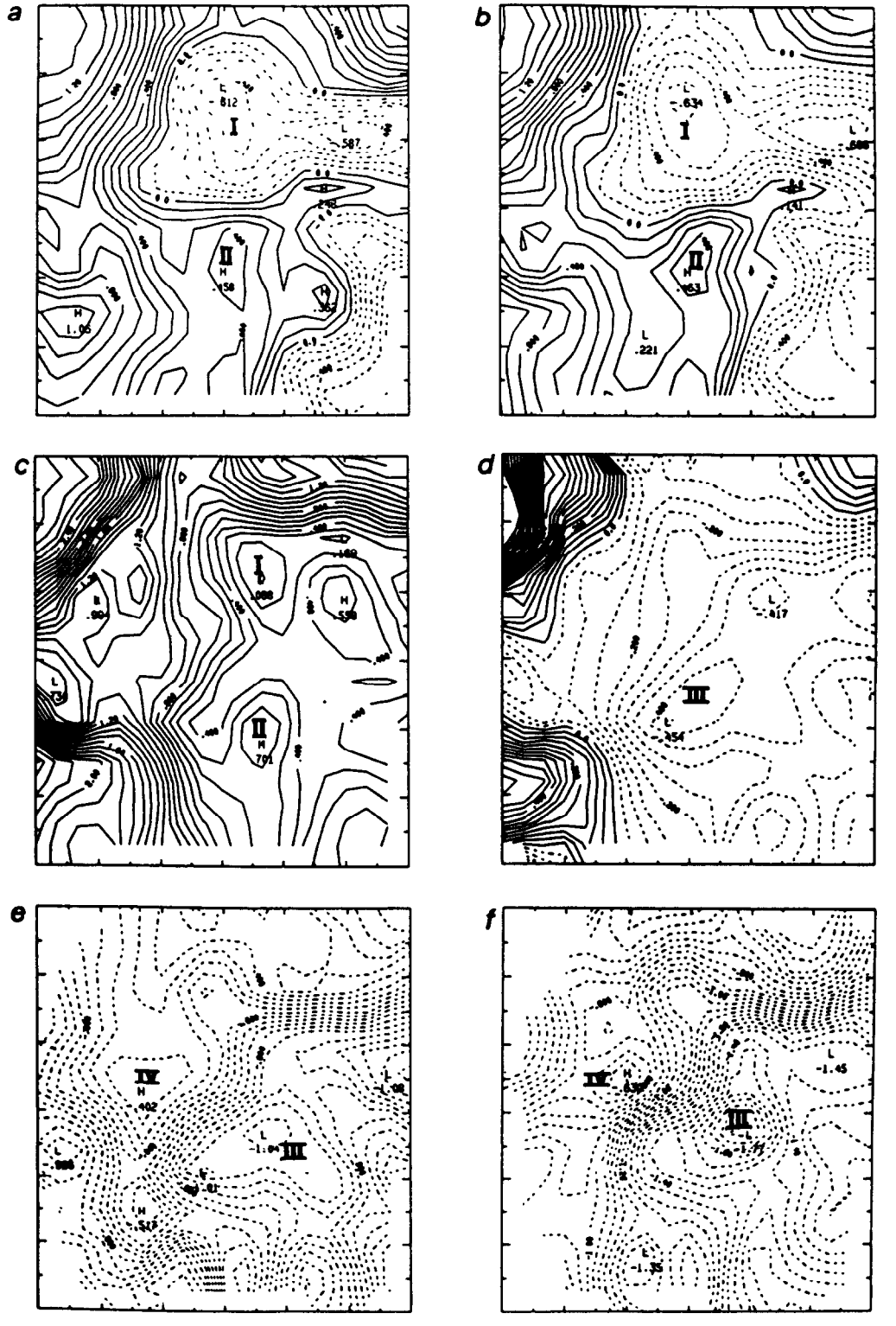
a
b
c
d
e
f

We have calculated the Brunt–Vaisala (N) frequency profile (Fig. 4) using only stations deeper than 100 m, so that our N is representative of the open ocean area. The profile has two relative maxima located just below the SW region and the LIW region, respectively. The enhanced stability of the region of SW is typical of the autumn season while the second maxima is probably indicative of the main thermocline layer of the region.

Using the quasigeostrophic vertical structure equation

$$\left(\frac{f_0^2}{N^2(z)}\psi_z\right)_z = \lambda^2\psi, \tag{1}$$

where ψ indicates the quasigeostrophic baroclinic modal function, the subscript indicates partial differentiation, $f_0 = 2\Omega \sin\theta_0$ is the Coriolis parameter evaluated at the central latitude of the domain of interest, $N^2(z)$ is the squared Brunt–Vaisala frequency profile of Fig. 4, λ^2 is the inverse of the squared Rossby radius of deformation, R, for each modal component. The results of the integration of equation (1) with $\psi_z = 0$ at $z = 0$ and $z = 250$ m are shown also in Fig. 4.

The first baroclinic mode has a zero crossing at 125 m and the correspondent Rossby radius of deformation is 5.4 km. The second baroclinic mode has a maximum at about 100 m and the zero crossings at 50 and 160 m. The second Rossby radius of deformation is 2.8 km. Such small values of R can be found only in the high latitude arctic regions (Emery *et al.*, 1984). Of course we consider these results to be representative only of the autumn stratification conditions, but they give between the highest values of the Rossby radii because of the enhanced vertical stratification during this season. As shown previously for other parts of the Mediterranean basin (Hecht *et al.*, 1988), the autumn season coincides with the largest values of N in the column of water. Furthermore, we know that in the winter season the temperature profiles are practically uniform with depth, so we expect the winter Rossby radii to have the lower bound local values. We point out again that these vertical modes and eigenvalues are representative of the open ocean part of our study area.

TEMPERATURE AND SALINITY MESOSCALE VARIABILITY

The temperature and salinity data have been objectively analysed by conventional methods (Bretherton *et al.*, 1976; Carter and Robinson, 1987) using an isotropic, homogeneous correlation function of the form:

$$C(r) = \left(1 - \frac{r^2}{a^2}\right)\exp\left(-\frac{r^2}{2b^2}\right); \quad r^2 = x^2 + y^2, \tag{2}$$

with the condition that $a \geq b\sqrt{2}$. Here x and y indicate longitudinal and latitudinal coordinates, respectively. The a coefficient corresponds to the zero crossing and $b\sqrt{2}$ is the e-folding scale of the correlation function. The values chosen for a and b are 30 and 20 km, respectively, because they are half the regional values found in the southeastern Levantine basin which has an internal first Rossby radius of deformation double ours. We

Fig. 5. Temperature anomalies, T', at several depths ($T' = T - T_a$). (a) 10 m, $T_a = 16.0$°C, contour interval (c.i.) 0.1°C; (b) 25 m, $T_a = 16.0$°C, c.i. = 0.1°C; (c) 40 m, $T_a = 14.5$°C, c.i. = 0.1°C, (d) 70 m, $T_a = 14.5$°C, c.i. = 0.05°C; (e) 100 m, $T_a = 14.5$°C, c.i. = 0.05°C, (f) 120 m, $T_a = 14.5$, c.i. = 0 05°C. The white, undrawn regions in the boxes correspond to expected error levels >40%

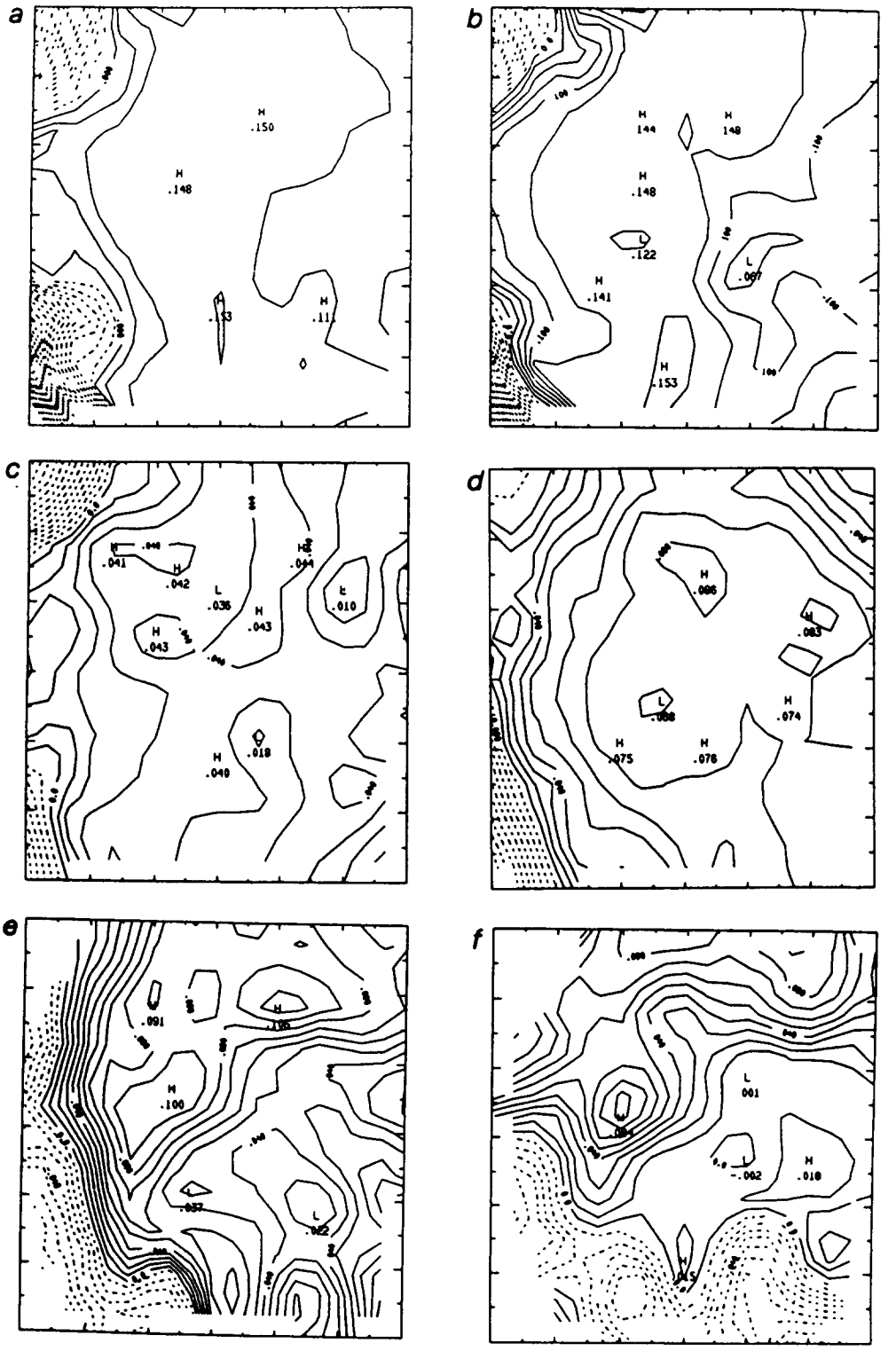
a
H
.150
H
.148
H
.11
b
H
144
H
148
H
.148
L
.122
L
.097
H
.141
H
.153
c
H
.041
H
.042
L
.036
H
.043
H
.043
H
.044
L
.010
H
.018
H
.040
d
H
.086
L
.083
L
.088
H
.074
H
.075
H
.078
e
H
.091
H
.100
L
.062
f
L
001
L
-.002
H
.018

also calculated the correlation function from the data, and these values seem reasonable. However the data scarcity and the anisotropy of the sampling pattern make the covariance matrix noisy, and we do not present it here.

The grid spacing for the interpolation is 5 km and the domain is 90×100 km^2 (Fig. 2). The expected error variance of the measurements is fixed to be 10%, and the objective analysis is carried out with 10 influential points. Parameter sensitivity experiments have shown that the objective analysis scheme is not very sensitive to larger values of influential points.

It is important to point out that our definition of eddy center is such that we have at least one closed contour at more than one level. The interpolated temperature anomaly fields are shown in Fig. 5. The temperature anomaly, T', is defined as the deviation of the temperature at that level, T, from a uniform reference temperature, T_a, e.g. $T' = T - T_a$.

The values of T_a were chosen to be representative of the SW layer ($T_a = 16$°C) and the average temperature of the LIW layer ($T_a = 14.5$°C). Naturally these T_a values are horizontal and vertical averages, and the single level values could depart positively or negatively at each depth.

The temperature anomalies show a very complicated pattern of jets and eddies with different horizontal scales and vertical extension. On the larger scales and at all levels we notice the presence of a thermal front along the northern and western sides of the area. This front divides the area into a coastal region and a deeper, open ocean region, separated approximately by the 100 m isobath contour line.

The surface temperature anomalies (10, 25 and 40 m in Fig. 5a–c) are characterized by two well defined eddies, indicated by I and II. The cyclonic eddy (I) is centered on the western Pomo depression and its major axis is about 30 km at 10 and 25 m, and only 15 km at 40 m. Its vertical structure is extremely baroclinic since it disappears at 70 m. The anticyclonic eddy (II) is also shallow but smaller with the maximum diameter of 15 km at 10 and 25 m.

The central LIW region temperature anomaly field (70 m) shows a totally different variability with smaller temperature gradients. We define only one eddy at this level, indicated by III in Fig. 5. Eddy III is vertically coherent with the 100 and 120 m levels.

The two lower levels (Fig. 5e,f) show an intensified jet between an anticyclonic (IV) and the cyclonic (III) eddy. The size of these eddies is about 15–20 km in diameter, and they are located south of the 200 m isobath that defines the western Pomo depression.

The salinity anomalies, S' (Fig. 6) are defined as the deviations of the salinity at that level, S, from a uniform reference salinity value, S_a, e.g. $S' = S - S_a$. These reference values were chosen to represent the minimum of the average salinities in the SW($S_a = 38.5$ PSU) and the minimum value in the LIW ($S_a = 38.6$ PSU).

The salinity field is dominated by the large gradients across the 100 m shelf break, especially at 10, 25 and 40 m. This salinity front coincides with the temperature front described before. Eddy-like structures have little correlation with the analogous temperature structures in the upper three levels, except for eddy IV at the LIW level. Eddy III is weak in its LIW signal as it is found rarely that cyclones have relevant LIW anomalies. It is

Fig 6 Salinity anomalies, S', at several depths ($S' = S - S_a$). (a) 10 m, S_a=38 5 PSU, contour interval (c.i) 0 05 PSU; (b) 25 m, S_a = 38.5 PSU, c.i =0 025 PSU; (c) 40 m, S_a= 38.5 PSU, c i.=0 01 PSU, (d) 70 m, S_a= 38 6 PSU, c i = 0 01 PSU; (e) 100 m, S_a = 38 6 PSU, c.i. = 0.01 PSU; (f) 120 m, S_a=38.6 PSU, c i = 0 01 PSU The white, undrawn regions in the boxes indicate expected error variance levels >40%

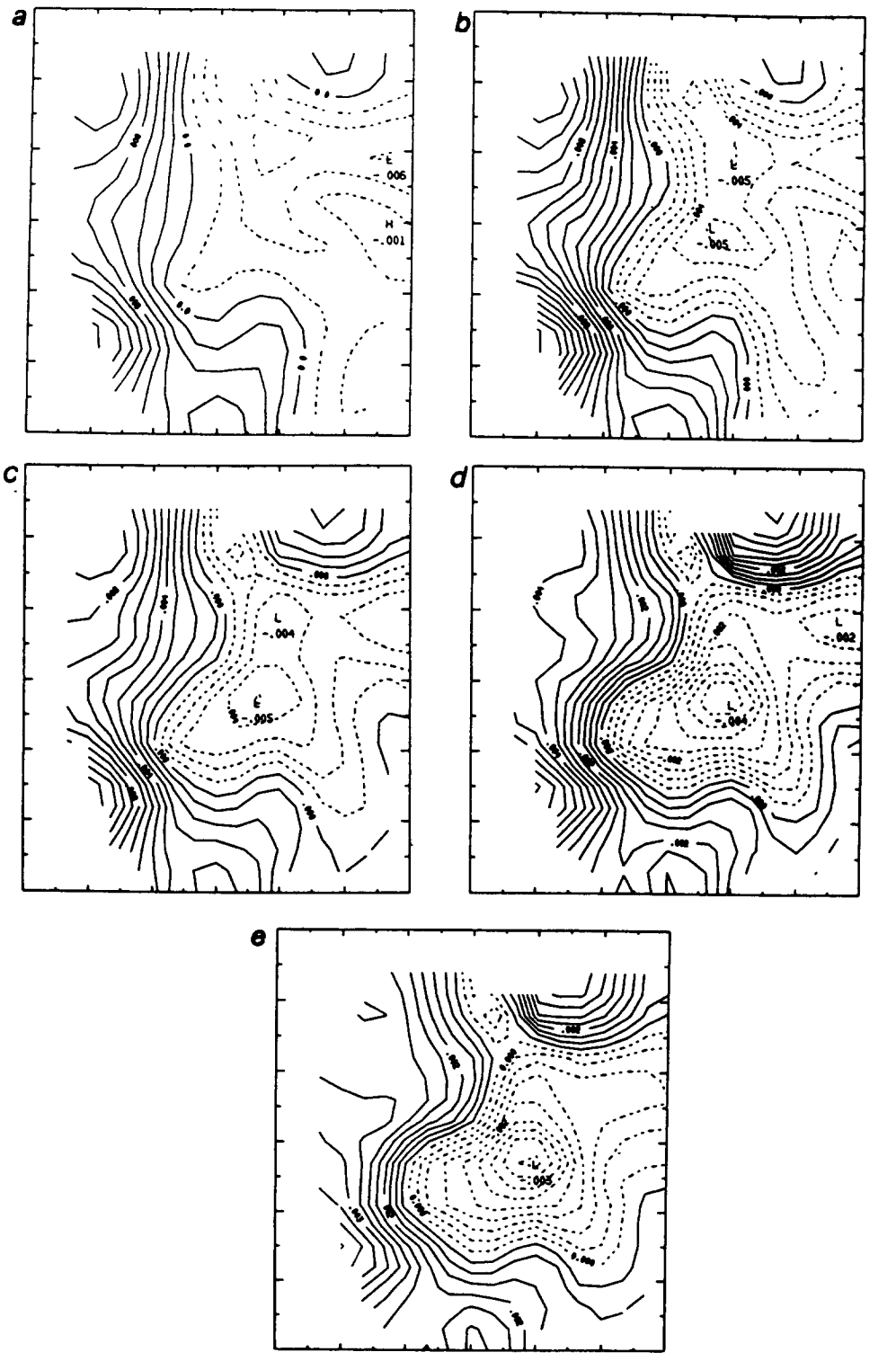
a
E
-.006
H
-.001
b
E
-.005
L
-.005
c
L
-.004
E
-.005
d
L
-.002
L
-.004
e
L
-.005

interesting to notice that eddy IV has both positive temperature and salinity anomalies, so that the net density contribution will be negligible. This is the fate of many LIW-intensified anticyclonic eddies that will disappear from the dynamic height field because of the opposite effect of temperature and salinity contributions in the equation of state.

The LIW abundance is confined in a tongue-like structure on the right side of the temperature frontal system (Fig. 5). This is consistent with the traditional view of the LIW transport in the basin: LIW enters the Adriatic from Otranto and follows the Yugoslavian coasts, turning cyclonically at the latitude of the Pomo depressions. Here we have shown that this cyclonic thermocline flow is strongly modulated by the mesoscale field. It assumes the structure of a tongue which insinuates around eddy centers. This vein of LIW embeds small eddy centers (10–15 km, Fig. 6e,f), which are shown by extrema in the salinity values. The eddy IV exhibits an extreme in the salinity tongue that starts in the northeast and turns southward.

DYNAMIC HEIGHT FIELDS

The dynamic height field relative to 140 m was analysed for 99 deep casts. This reference level was chosen because it marks the upper end of the DW layer of Fig. 3 and it is shallow enough to have an acceptable number of stations for the mapping.

The dynamic height field (Fig. 7) shows that the surface flow is dominated by a southward meandering jet and in the thermocline levels a single eddy center occupies the region with an intensified jet at its border. The southward jet can be connected at the northern border of the domain with a piece of westward jet probably meandering around another eddy outside our study area. The jet bifurcates around the southern border of the cyclonic eddy, one branch following its path south and the other turning eastward and intensifying the southern border of the eddy.

The subsurface-intensified cyclonic eddy is located on the negative temperature anomaly of eddy III and on the southern side of the western Pomo depression. It has a very symmetric core of about 25 km of diameter at the thermocline levels and it shows a double center at the upper levels (Fig. 7b,c). We expect the topography to be important to set the location and the persistence in time of the eddy in this region. All the other temperature eddies have disappeared due to compensating effects between the salinity and temperature anomalies.

The intensification of this eddy at 70 and 100 m (Fig. 7d,e) suggests that an important vertical modal component of the eddy field is second baroclinic. The first baroclinic mode (see Fig. 4) has a zero crossing of about 120 m, and the second baroclinic mode reaches its maximum amplitude at 100 m. Thus this eddy field shows unequivocably a second baroclinic component; we believe this is evidence of second baroclinic intensified eddies that seem to be common in the eastern Mediterranean Sea (Hecht *et al.*, 1988). The eddy diameter is thus about 5 times the first baroclinic Rossby radius of deformation, as much as in the North Atlantic where the baroclinic eddies have a diameter of about 5 times the first Rossby radius of deformation.

Fig 7 Dynamic height anomaly fields at (a) 10, (b) 25, (c) 40, (d) 70 and (e) 100 m; referred to 140 m. The average values subtracted and contour intervals (c i.) are respectively: (a) −0.098 m, c.i = 0.002 m, (b) −0.092 m, c.i. = 0.001 m; (c) −0.085 m, c.i. = 0.001 m; (d) −0 063 m, c i. = 0.0005 m; (e) −0 038 m; c i. = 0 0005 m The white, undrawn areas correspond to expected error variance levels >40%

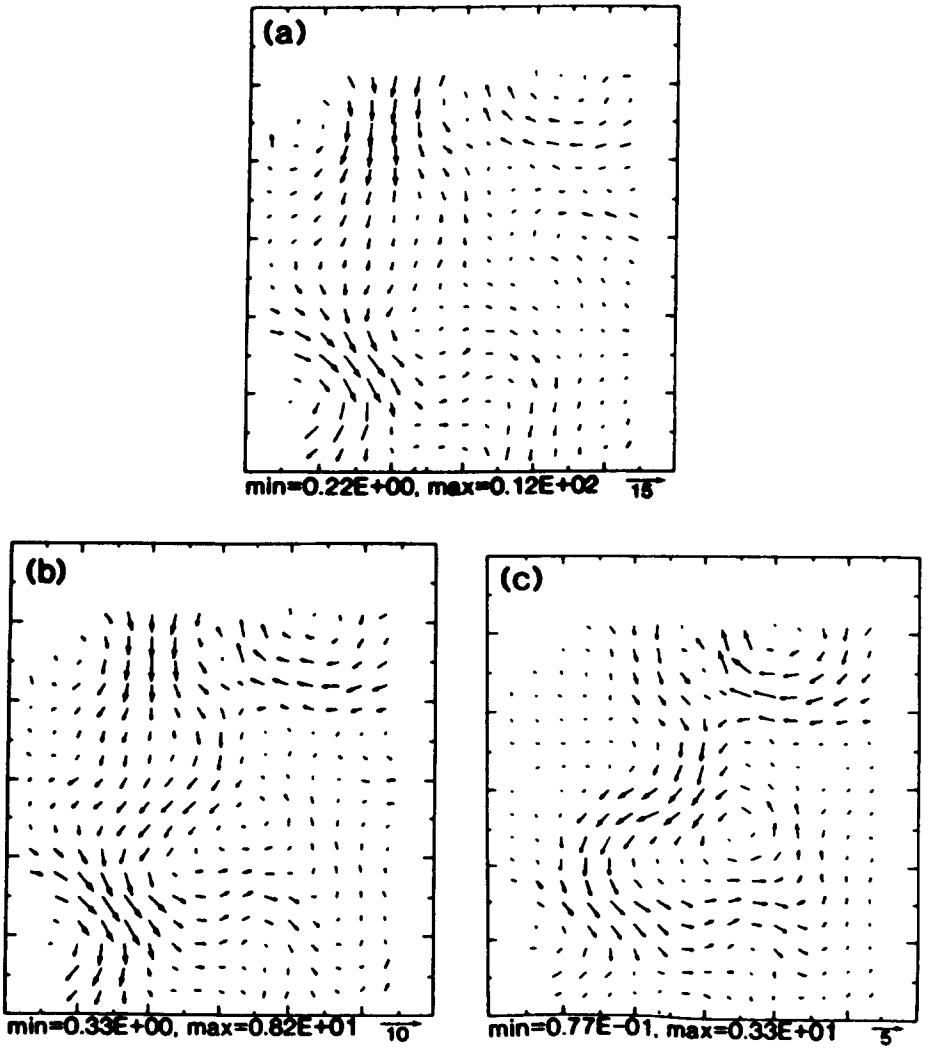

Fig 8. Geostrophic velocity arrows in cm s^{-1} at (a) 10, (b) 40 and (c) 100 m of depth. The minimum, maximum (min, max) of the field is indicated on the bottom of each picture together with a reference arrow

Finally, the baroclinic geostrophic velocities calculated from the dynamic height fields (Fig. 8) show that the upper themocline levels velocities (calculated with respect to the no motion level at 140 m) are of the order of 10 cm s^{-1} or slightly less. This velocity field suggests the intensification of segments of the jet-frontal structure (Fig. 8a,b), the complex branching of the southward directed jet, and the thermocline intensified flow of the cyclonic eddy (compare Fig. 8b with Fig. 8c).

Acknowledgements—We would like to thank the crew of the R V. *S. Lo Bianco* Many thanks to Dr Mariella Morbidoni for assistance in the data gathering phase of the experiment This work has been supported by a grant given to CNR by the Progetto Strategico Oceanografia e Tecnologie Marine

REFERENCES

ARTEGIANI A and E SALUSTI (1987) Field observations of the flow of dense water on the bottom of the Adriatic Sea during winter of 1981 *Oceanologica Acta*, **10**, 387–391

ARTEGIANI A , R AZZOLINI, E PASCHINI and M MORBIDONI (1987) Mesoscale variability in the Middle Adriatic Sea *Terra Cognita*, **7**, 1–543

ARTEGIANI A , R AZZOLINI and E SALUSTI (1989) On the dense water in the Adriatic Sea *Oceanologica Acta*, **12**, 151–160

BRETHERTON F P , R E DAVIS and C B FANDRY (1976) A technique for objective analysis and design of oceanographic experiments. *Deep-Sea Research*, **23**, 559–582

CARTER E F and A R ROBINSON (1987) Analysis models for the estimation of oceanic fields *Journal of Atmospheric Oceanic Technology*, **4**, 49–74

EMERY W J , W G. LEE and L. MAGAARD (1984) Geographic and seasonal distribution of Brunt–Vaisala frequency and Rossby radii in the North Pacific and the North Atlantic *Journal of Physical Oceanography*, **14**, 294–317

FRANCO P (1972) Oceanography of the Northern Adriatic Sea—2 Hydrologic features· cruises January–February and April–May 1966. *Archives of Oceanography and Limnology, Suppl.*, **17**, 1–97

FRANCO P , L JEFTIC, P MALANOTTE-RIZZOLI, A MICHELATO and M. ORLIC (1982) Descriptive model of the Northern Adriatic *Oceanologica Acta*, **5**, 379–389

HECHT A , N PINARDI and A R. ROBINSON (1988) Current, water masses, eddies and jets in the Mediterranean Levantine basin *Journal of Physical Oceanography*, **18**, 1320–1353

HENDERSHOTT M C and P RIZZOLI (1972) The winter circulation of the Adriatic Sea. *Deep-Sea Research*, **23**, 353–373

MALANOTTE-RIZZOLI P and A. BERGAMASCO (1983) The dynamics of the coastal region of the Adriatic Sea *Journal of Physical Oceanography*, **13**, 1105–1130

MOOERS C N K and A. R. ROBINSON (1984) Turbulent jets and eddies in the California current and inferred cross-shore transports *Science* **223**, 51–53

OVCHINNIKOV I M. (1984) The formation of intermediate water in the Mediterranean *Oceanology*, **24**, 168–173

OVCHINNIKOV I M , V I ZATS, V G KRIVOSHEYA, M S NEMIROVSKY and A I UDODOV (1987) Winter convection in the Adriatic and formation of deep eastern Mediterranean waters *Annales Geophysicae*, **5**, 89–92

OZSOY E., A HECHT and U. UNLUATA (1989) Circulation and hydrology of the Levantine Basin. Results of POEM coordinated experiments 1985–1986 *Progress in Oceanography*, **22**, 125–170

POLLAK M J. (1951) The sources of deep water of the eastern Mediterranean Sea. *Journal of Marine Research*, **10**, 128–152

ROBINSON A. R., A HECHT, N. PINARDI, J. BISHOP, W. G LESLIE, Z ROSENTROUB, A J MARIANO and S BRENNER (1987) Small synoptic/mesoscale eddies and energetic variability of the Eastern Levantine basin *Nature*, **327**, 131–134

UNESCO (1988) The acquisition, calibration and analysis of CTD data Technical papers in Marine Science, 54

ZORE-ARMANDA M (1956) On gradient currents in the Adriatic Sea *Acta Adriatica*, **8**, 1–38

ZORE-ARMANDA M. (1963) Les masses d'eaux de la mer Adriatique. *Acta Adriatica*, **10**, 1–94

ZORE-ARMANDA M. and M. GACIC (1987) Effects of bura on the circulation in the North Adriatic *Annales Geophysicae*, **5**, 93–102